# Correlation-Driven Insulator-Metal Transition in Near-Ideal Vanadium Dioxide Films

A. X. Gray, J. Jeong, N. P. Aetukuri, P. Granitzka, Z. Chen, R. Kukreja, D. Higley, T. Chase, A. H. Reid, H. Ohldag, M. A. Marcus, A. Scholl, A. T. Young, A. Doran, C. A. Jenkins, P. Shafer, E. Arenholz, M. G. Samant, S. S. P. Parkin, and H. A. Dürr

Phys. Rev. Lett. **116**, 116403 — Published 18 March 2016

DOI: 10.1103/PhysRevLett.116.116403

# Correlation-driven insulator-metal transition in near-ideal vanadium dioxide films

A. X. Gray[1,2⋆], J. Jeong[3], N. P. Aetukuri[3], P. Granitzka[1,4], Z. Chen[1,5], R. Kukreja[1,6], D. Higley[1,7], T. Chase[1,7], A. H. Reid[1], H. Ohldag[8], M. A. Marcus[9], A. Scholl[9], A. T. Young[9], A. Doran[9], C. A. Jenkins[9], P. Shafer[9], E. Arenholz[9], M. G. Samant[3], S. S. P. Parkin[3] and H. A. Dürr[1⋆]

[1]Stanford Institute for Materials and Energy Sciences, SLAC National Accelerator Laboratory, 2575 Sand Hill Road, Menlo Park, California 94025, USA

[2]Department of Physics, Temple University, 1925 N. 12th St., Philadelphia, Pennsylvania 19130, USA

[3]IBM Almaden Research Center, 650 Harry Road, San Jose, California 95120, USA

[4]Van der Waals-Zeeman Institute, University of Amsterdam, 1018XE Amsterdam, The Netherlands

[5]Department of Physics, Stanford University, Stanford, California 94305, USA

[6]Department of Materials Science and Engineering, Stanford University, Stanford, California 94305, USA

[7]Department of Applied Physics, Stanford University, Stanford, California 94305

[8]Stanford Synchrotron Radiation Lightsource, SLAC National Accelerator Laboratory, 2575 Sand Hill Road, Menlo Park, California 94025, USA

[9]Advanced Light Source, Lawrence Berkeley National Laboratory, One Cyclotron Road, Berkeley, California 94720, USA

⋆email: axgray@temple.edu, hdurr@slac.stanford.edu

## Abstract

We use polarization- and temperature-dependent x-ray absorption spectroscopy, in combination with photoelectron microscopy, x-ray diffraction and electronic transport measurements, to study the driving force behind the insulator-metal transition in $VO_2$. We show that both the collapse of the insulating gap and the concomitant change in crystal symmetry in homogeneously strained single-crystalline $VO_2$ films are preceded by the purely-electronic softening of Coulomb correlations within V-V singlet dimers. This process starts 7 K (±0.3 K) below the transition temperature, as conventionally defined by electronic transport and x-ray diffraction measurements, and sets the energy scale for driving the near-room-temperature insulator-metal transition in this technologically-promising material.

A clear understanding of how new electronic and structural phases of matter arise and evolve is not only important for basic science but is also becoming crucial for information technology. Our ability to navigate and ultimately control the complex dynamical pathways in the multidimensional landscape of the electronic, spin, and lattice degrees of freedom is starting to play a critical role in achieving technical feasibility and efficient performance of future electronic devices [1].

One of the prime material candidates for such devices, vanadium dioxide ($VO_2$), undergoes an insulator-metal transition with a four-orders-of-magnitude increase in conductivity and a concomitant monoclinic-rutile structural transformation accompanied by the dimerization of neighboring vanadium atoms just above room temperature [2]. This makes $VO_2$ suitable for technological applications, from solid-state sensors and optical detectors to field-effect transistors and memristors [1], and motivates investigations aimed at controlling the insulator-metal transition by external stimuli [3-7] and epitaxial strain [8].

The nature of the driving force behind the insulator-metal transition in this strongly-correlated electron system is one of the longest-standing problems in condensed matter physics [2]. Both electron-electron correlations and electron-lattice interactions are believed to be relevant. However, the question of which drives the other and the interplay between Mott-Hubbard [9,10] and Peierls [11,12] mechanisms remain under debate [13-18].

The structural and electronic dichotomy of the insulator-metal transition in $VO_2$, depicted schematically in Fig. 1, opens the door for two possible explanations as to what could be the driving force and the physical mechanism behind this phenomenon. On one hand, a structural transformation with strong dimerization (Figs. 1(a),(c)) presents seemingly convincing evidence for the Peierls-like picture, wherein opening of the insulating gap shown schematically in Fig. 1(d) is caused by the lattice distortion [11,12]. On the other hand, the evidence of strong electron-electron correlation effects suggests the Mott-Hubbard scenario in which strong Coulomb interaction between electrons plays the key role in triggering the insulator-metal transition by splitting the near-Fermi-level electronic states (Fig. 1(b)) into the bonding and anti-bonding bands, thus opening-up an insulating gap (Fig. 1(d)) [9,10]. To this day,

however, the underlying physics of the transition remains elusive due to the lack of success in consolidating all of its experimentally observed structural and electronic aspects in a singular self-consistent quantitative theoretical picture [9-17]. A further complication arises due to phase separation scenarios often accompanying insulator-metal transitions [19-21]. In bulk-like $VO_2$ films the coexistence of insulating and metallic-like patches was observed in various experiments probing electronic and structural aspects [19,20]. Similarly, in thick epitaxial films the formation of unidirectional metallic-like stripes [21] and a monoclinic-like metallic phase [22] was observed in the vicinity of the transition.

Here we show that near-ideal, high-quality ultrathin epitaxial $VO_2$ films grown on $TiO_2$(001) substrates display a spatially homogeneous insulator-metal transition without phase segregation. We track the $VO_2$ insulator-metal transition by monitoring with polarization-dependent x-ray absorption spectroscopy (XAS) spectroscopic features of the dimer V-V electronic correlations (Fig. 2d), the electronic band gap (Fig. 2c) and the dimer V-V Peierls lattice distortion (Fig. 2d), respectively. This enables the unambiguous assignment of the insulator-metal transition to two consecutive processes occurring with increasing temperature. Initially, the insulating phase is modified by a weakening of electronic correlations in dimer V-V singlet states [18]. This process sets in as much as 7 K (±0.3 K) below the proper insulator-metal transition temperature ($T_{IMT}$ = 295±0.3 K) probed by the electronic band gap collapse. The gap collapse starts as soon as the V-V singlet correlations have completely disappeared at $T_{IMT}$. Only at $T_{IMT}$ do we detect structural changes in V-V dimerization as implied by a Peierls scenario, as well as electronic changes consistent with the disappearance of a dimer V-V Peierls lattice distortion [23].

For our experiment, 10 nm thick high-quality single-crystalline $VO_2$ thin films were grown epitaxially on single-crystalline $TiO_2$(001) substrates by pulsed laser deposition, following the procedures described in-depth in Refs. 5 and 8 (our prior studies). This results in coherently-strained $VO_2$(001) films with a $c_R/a_R$ lattice-constant ratio of 0.617 [8]. The films undergo an abrupt insulator-metal transition at 295 K upon heating that is accompanied by a change in crystal symmetry. This transition is sharper than that

observed for comparable films [22] and indicative of the absence of any detectable electronic phase separation [23].

High-angular-resolution (<0.01°) temperature-dependent XRD measurements of the $VO_2/TiO_2(001)$ films were carried out in a vacuum of ~1 mTorr, using a Bruker D8 Discover system equipped with variable-temperature stage enclosed in an x-ray transparent beryllium dome. Fig. 1(e) shows two typical θ-2θ scans across the $TiO_2$ substrate (002) and the $VO_2$ film peaks, which are indexed as $(002)_R$ for the high-temperature rutile phase, and $(\bar{4}02)_M$ for the low-temperature monoclinic phase. The scans were collected immediately below and above the insulator-metal transition, and show an abrupt change of the out-of-plane inter-planar spacing in the $VO_2$ film at the transition temperature $T_{IMT}$=295K (green circles in the inset). Concomitant in-situ electronic transport measurements (purple circles in the inset) confirm that the insulator-metal transition and the structural monoclinic-rutile transition occur at the same temperature.

Temperature- and x-ray polarization-dependent XAS measurements were carried out at the elliptically polarized undulator beamline 4.0.2 of the Advanced Light Source, using the *Vector Magnet* endstation equipped with a 4-axis sample manipulator with cryogenic cooling as well as conductive heating capabilities [24]. The nearly 100% linearly-polarized x-ray beam was focused down to 100 μm diameter spot at the sample surface. Average probing depth in the total electron yield XAS detection mode was estimated to be about 5 nm, providing bulk-sensitive information with minimal contribution from surface adsorbates. The temperature was varied using a closed-loop feedback-activated temperature controller, providing temperature stability of ±0.1 K. Measurements were carried out at several locations on the sample, to exclude the possibility of x-ray sample damage.

Figure 2 shows high-resolution polarization-dependent XAS measurements at the O *K* edge. O *K* edge XAS probes the O 2*p*-projected unoccupied density of states resulting from dipole-allowed x-ray transitions from the 1*s* core shell. It is well known [27-29] that this provides access to all relevant states in the unoccupied $VO_2$ conduction band via O 2*p* - V *3d* orbital hybridization. We use the x-ray polarization dependence of XAS to determine the orbital symmetry. In the grazing incidence experimental geometry

shown in Fig. 2(a), linearly polarized x-rays with the electric-field orientation parallel to the $c_R$ axis (E ∥ $c_R$) preferentially probe the unoccupied $d_{\|}$ states of $a_{1g}$ symmetry. $d_{\|}$ orbitals are preferentially oriented along the $c_R$ direction (see Fig. 2(b)). X-rays with their electric-field orientation perpendicular to the $c_R$ axis (E ⊥ $c_R$) are more sensitive in probing the states with $e_g^{\pi}$ symmetry, comprised of $d_{xz}$ and $d_{yx}$ orbitals ($\pi$* states) (see Fig. 2(b)) [8, 27].

Figure 2(c) shows typical temperature and polarization-dependent O XAS spectra for the $VO_2$ film, as measured for the photon energy range between 528 and 531 eV. The spectra have been normalized to equal edge jump accounting for the incomplete alignment of x-ray polarization with the $d_{\|}$ orbital orientation and the varying orbital multiplicity for the two polarizations [27,30]. The leading edge found at 528.7 eV (in the insulating phase) is known to sensitively probe the closing of the electronic band gap with increasing temperature [27]. This is observed as the edge shift to lower photon energy with increasing temperature which is one of the major effects seen in Fig. 2(c) especially between spectra taken with fixed x-ray polarization. Overlaid with this change in band gap are polarization effects seen in the insulating phase but not for metallic $VO_2$. Two most prominent polarization-dependent differences are observed at the photon energies of 528.7 eV and 530.2 eV (see also Fig. 2(d)) and are related to the dimer V-V electronic correlations and Peierls lattice distortion, respectively. We will first describe these three spectroscopic features in Figs. 2(c) and 2(d) before proceeding to the temperature dependence.

The XAS spectra measured at the temperature of 310 K, well above the insulator-metal transition ($T_{IMT}$=295 K), are shown in Fig. 2(c) as open and solid red symbols. These spectra are good representations of the metallic unoccupied density of states immediately above the Fermi level [8,31]. Consistent with prior experimental results [27] and theoretical calculations [18] no significant difference between the spectra collected using two mutually-orthogonal x-ray linear polarizations is observed due to an almost isotropic distribution of the $t_{2g}$ orbitals near the Fermi level [18,30].

The insulating-state spectra (shown in blue) collected at 280 K (15 K below the insulator-metal transition) are shifted by about 80-100 meV to higher photon energy due to the opening of the insulating

gap and, in stark contrast with the metallic-state spectra, are significantly different. Their intensity difference plotted in Fig. 2(d) features two major polarization-dependent peaks favoring E ∥ $c_R$ polarization. The more prominent peak centered at the photon energy of 530.2 eV is a well-known $d_{\parallel}$ state arising from the Peierls distortion of the lattice [13,18,27]. This $d_{\parallel}$ *Peierls* peak is depicted schematically (red outline) in Fig. 1(d). The second feature is observed at the photon energy of 528.7 eV. Such additional XAS intensity for E ∥ $c_R$ presents direct evidence of the additional $d_{\parallel}$ orbital character at the onset of the conduction band (depicted schematically in Fig. 1(d)) which has been identified as the fingerprint of the strong electronic correlations within the V-V dimers [18,27]. In addition to being present in the spectra for the coherently-strained thin $VO_2$(001) films, such a $d_{\parallel}$ V-V singlet state has also been observed for the bulk $VO_2$ single-crystals [27]. It represents a unique feature of the strongly-correlated insulating phase of crystalline $VO_2$ [23].

The temperature dependence of the electronic band gap (red solid symbols in Fig. 3(a)) displays the insulator metal transition with $T_{IMT}$ = 295±0.3 K. This insulator-metal transition is closely tracked by the monoclinic-rutile structural transition monitored by the dimer V-V Peierls peak (yellow solid symbols in Fig. 3(a)). Extended datasets with individual spectra for each temperature are presented in Fig. S1 of [23]. Interestingly, the temperature dependence of the dimer V-V singlet state is very different (blue/white symbols in Fig. 3(a)). We observe that the V-V state intensity (as defined in Fig. 2(d)) begins to decay at 288 K which is 7 K below $T_{IMT}$. The dimer V-V singlet state disappears completely just before the onset of the electronic band gap collapse at 294 K. Thus, our results strongly suggest that the insulator-metal transition in $VO_2$ follows a three-stage pathway depicted schematically in Figs. 3(b)-(d). **(1)** At temperatures that are up to 7 K below the insulator-metal transition (denoted $T \ll T_{IMT}$ in Fig. 3(a)), $VO_2$ is in the insulating monoclinic phase, with two $3d^1$ electrons of two adjacent dimer V-V atoms forming a strongly-correlated singlet state of $d_{\parallel}$ symmetry [18] (Fig. 3(b)). **(2)** Upon heating above $T_{IMT}$-7K, $VO_2$ remains in the insulating monoclinic state, i.e. the electronic band gap remains unchanged as demonstrated by the upper band gap edge shown in Fig. 3(a). However, the electronic correlations start to soften, as evidenced by the decay of the dimer V-V singlet state intensity (Fig. 3(c)). **(3)** Finally, once the

electronic correlations are sufficiently diminished, the band gap collapse is initiated. This latter process is accompanied by the change in crystal symmetry from insulating monoclinic to metallic rutile as evidenced by the dimer V-V Peierls peak change (Fig. 3(d)). Above 297 K $VO_2$ is in a homogeneous metallic state. Process **(3)** seems to correspond to the conventional Peierls mechanism where lattice distortions keep the band gap intact. However, our results show that it is the preceding decay of electron correlations giving rise to dimer V-V singlet state that set the high-temperature energy scale in $VO_2$. As an important consequence of this transition pathway, one can define a second distinct critical temperature ($T_{corr}$=290 K ± 0.3 K) at which $VO_2$ undergoes a purely-electronic transition between a strongly-correlated and a conventional monoclinic Peierls insulator. This transition temperature $T_{corr}$ is 5 K (± 0.3 K) below the insulator-metal transition.

A temperature- and polarization-dependent spectro-microscopic investigation of the sample using photoemission microscopy (PEEM) at the O *K* absorption edge (528.7 eV) reveal that our thin coherently-strained $VO_2$ film grown in (001) crystallographic orientation on a single-crystalline $TiO_2$ substrate does not undergo any detectable insulator/metal phase segregation across the insulator-metal transition [23]. Indirectly, such quasi-instantaneous single-domain switching is evidenced by the sharpness of the transition (2-4 K width) observed in the electronic structure via XAS (Fig. 3(a)) and electronic transport measurements, as well as structurally via x-ray diffraction spectroscopy (Fig 1(e)). This is in stark contrast to bulk-like films where epitaxial strain is fully relaxed. We find that such films do display a separation into metallic and insulating regions during the insulator-metal transition as shown in Fig. S3 of [23].

As a consequence of such inhomogeneous transition, fully-relaxed bulk-like films exhibit a broader IMT as measured via area-averaging spectroscopic techniques such as XAS. Nevertheless, similar to the fully-strained film, the collapse of the gap in the fully-relaxed bulk-like film is still preceded by the softening of Coulomb correlations within V-V singlet dimers occurring at a lower temperature $T_{corr}<T_{IMT}$ [23]. This suggests that the IMT pathway depicted schematically in Figs. 3(b)-(d) is ubiquitous for a wide range of strains and thicknesses.

In summary, our results indicate that the temperature-driven insulator-metal transition in a strongly-correlated oxide $VO_2$ is preceded and, possibly, driven by the purely-electronic phase transition occurring at a lower temperature ($T_{corr}<T_{IMT}$). We have observed the emergence and the temperature-dependent evolution of the new intermediate monoclinic/insulating phase in $VO_2$ which is characterized by softening and disappearance of the strong correlations within the V-V dimers. These findings have a far-reaching impact on our understanding of the complex physics of the insulator-metal transition in strongly-correlated oxides, since they suggest that the fundamental electronic and structural transformations in these materials arise from *precursory* changes in the electronic correlations. Thus, for all the future practical applications of $VO_2$ as a building-block for next-generation electronic devices, as well as for a wide range of time-resolved pump-probe experiments, this underpinning transition and the characteristic $T_{corr}$ should be carefully characterized and understood.

Research at Stanford was supported through the Stanford Institute for Materials and Energy Sciences (SIMES) under contract DE-AC02-76SF00515 and the LCLS by the US Department of Energy, Office of Basic Energy Sciences. The Advanced Light Source is supported by the Director, Office of Science, Office of Basic Energy Sciences, US Department of Energy under Contract No. DE-AC02-05CH11231. The Stanford Synchrotron Radiation Lightsource, SLAC National Accelerator Laboratory, is supported by the Director, Office of Science, Office of Basic Energy Sciences, US Department of Energy under Contract No. DE-AC02-76SF00515. Authors would like to thank C.-C Chen, B. Moritz, T. P. Devereaux and M. van Veenendaal for helpful discussions.

## References


1. Z. Yang, C. Ko, and S. Ramanathan, Annu. Rev. Mater. Res. **41**, 337 (2011).
2. F. J. Morin, Phys. Rev. Lett. **3**, 34 (1959).
3. A. Cavalleri, Cs. Tóth, C. W. Siders, J. A. Squier, F. Ráksi, P. Forget, and J. C. Kieffer, Phys. Rev. Lett. **87**, 237401 (2001).
4. M. K. Liu, H. Y. Hwang, H. Tao, A C. Strikwerda, K. Fan, G. R. Keiser, A. J. Sternbach, K. G. West, S. Kittiwatanakul, J. Lu, S. A. Wolf, F. G. Omenetto, X. Zhang, K. A. Nelson, and R. D. Averitt, Nature **487**, 345 (2012).
5. J. Jeong, N. P. Aetukuri, T. Graf, T. D. Schladt, M. G. Samant, and S. S. P. Parkin, Science **339**, 1402 (2013).
6. C. Marini, M. Bendele, B. Joseph, I. Kantor, M. Mitrano, O. Mathon, M. Baldini, L. Malavasi, S. Pascarelli, and P. Postorino, Europhys. Lett. **108**, 36003 (2014).
7. L. Bai, Q. Li, S. A. Corr, Y. Meng, C. Park, S. V. Sinogeikin, C. Ko, J. Wu, and G. Shen, Phys. Rev. B **91**, 104110 (2015).
8. N. B. Aetukuri, A. X. Gray, M. Drouard, M. Cossale, L. Gao, A. H. Reid, R. Kukreja, H. Ohldag, C. A. Jenkins, E. Arenholz, H. A. Dürr, M. Samant, and S. S. P. Parkin, Nature Physics **9**, 661 (2013).
9. A. Zylberstejn and N. F. Mott, Phys. Rev. B **11**, 4383 (1975).
10. T. M. Rice, H. Launois, and J. P. Pouget, Phys. Rev. Lett. **73**, 3042 (1994).
11. D. Adler and H. Brooks, Phys. Rev. **155**, 826 (1967).
12. R. M. Wentzcovitch, W. Schulz, and P. Allen, Phys. Rev. Lett. **72**, 3389 (1994).
13. J. B. Goodenough, J. Solid State. Chem. **3**, 490 (1971).
14. J. P. Pouget, H. Launois, T. M. Rice, P. Dernier, A. Gossard, G. Villeneuve, and P. Hagenmuller, Phys. Rev. B **10**, 1801 (1974).
15. J. P. Pouget, H. Launois, J. P. D'Haenens, P. Merenda, and T. M. Rice, Phys. Rev. Lett. **35**, 873 (1975).
16. A. Bianconi, Phys. Rev. B **26**, 2741 (1982).

17. V. Eyert, Ann. Phys. (Leipzig) **11**, 648 (2002).

18. S. Biermann, A. Poteryaev, A. I. Lichtenstein, and A. Georges, Phys. Rev. Lett. **94**, 026404 (2005).

19. M. M. Qazilbash, M. Brehm, B.-G. Chae, P.-C. Ho, G. O. Andreev, B.-J. Kim, S. J. Yun, A. V. Balatsky, M. B. Maple, F. Keilmann, H.-T. Kim, and D. N. Basov, Science **318**, 1750 (2007).

20. M. M. Qazilbash, A. Tripathi, A. A. Schafgans, B.-J. Kim, H.-T. Kim, Z. Cai, M. V. Holt, J. M. Maser, F. Keilmann, O. G. Shpyrko, and D. N. Basov, Phys. Rev. B **83**, 165108 (2011).

21. M. K. Liu, M. Wagner, E. Abreu, S. Kittiwatanakul, A. McLeod, Z. Fei, M. Goldflam, S. Dai, M. M. Fogler, J. Lu, S. A. Wolf, R. D. Averitt, and D. N. Basov, Phys. Rev. Lett. **111**, 096602 (2013).

22. J. Laverock, S. Kittiwatanakul, A.□A. Zakharov, Y.□R. Niu, B. Chen, S.□A. Wolf, J.□W. Lu, and K.□E. Smith, Phys. Rev Lett. **113**, 216402 (2014).

23. See Supplemental Material at http://link.aps.org/supplemental/##### for details related to characterization of the samples mentioned in the letter, as well as some expanded temperature-dependent XAS and PEEM datasets detailing the results shown in the main text.

24. A. T. Young, E. Arenholz, J. Feng, H. Padmore, S. Marks, R. Schlueter, E. Hoyer, N. Kelez, and C. Steier, Surf. Rev. Lett. **9**, 549 (2002).

25. S. Shin, S. Suga, M. Taniguchi, M. Fujisawa, H. Kanzaki, A. Fujimori, H. Daimon, Y. Ueda, K. Kosuge, and S. Kachi, Phys. Rev. B **41**, 4993 (1990).

26. S. Suga, A. Sekiyama, S. Imada, T. Miyamachi, H. Fujiwara, A. Yamasaki, K. Yoshimura, K. Okada, M. Yabashi, and K. Tamasaku, New J. Phys. **11**, 103015 (2009).

27. T. C. Koethe, Z. Hu, M. W. Haverkort, C. Schüßler-Langeheine, F. Venturini, N. B. Brookes, O. Tjernberg, W. Reichelt, H. H. Hsieh, H.-J. Lin, C. T. Chen, and L. H. Tjeng, Phys. Rev. Lett. **97**, 116402 (2006).

28. F. M. F. de Groot, M. Grioni, J. C. Fuggle, J. Ghijsen, G. A. Sawatzky, and H. Petersen, Phys. Rev. B **40**, 5715 (1989).

29. M. Abbate, F. M. F. de Groot, J. C. Fuggle, Y. J. Ma, C. T. Chen, F. Sette, A. Fujimori, Y. Ueda, and K. Kosuge, Phys. Rev. B **43**, 7263 (1991).

30. M. W. Haverkort, Z. Hu, A. Tanaka, W. Reichelt, S. V. Streltsov, M. A. Korotin, V. I. Anisimov, H. H. Hsieh, H.-J. Lin, C. T. Chen, D. I. Khomskii, and L. H. Tjeng, Phys. Rev. Lett. **95**, 196404 (2005).
31. N. F. Quackenbush, J. W. Tashman, J. A. Mundy, S. Sallis, H. Paik, R. Misra, J. A. Moyer, J.-H. Guo, D. A. Fischer, J. C. Woicik, D. A. Muller, D. G. Schlom, and L. F. J. Piper, Nano Lett. **13**, 4857 (2013).

## Figure Legends

**FIG. 1.** **(a)** In the high-temperature ($T>T_{IMT}$) metallic phase $VO_2$ forms rutile lattice structure with $P4_2/mnm$ space symmetry where V atoms (yellow) occupy centers of six-fold oxygen-coordinated sites (O atoms not shown). **(b)** The near-Fermi-level $t_{2g}$ states are separated in energy by the orthorhombic component of the crystal field into the twofold-degenerate $e_g^{\pi}$ ($\pi^*$) states and a single $a_{1g}$ orbital, which is aligned parallel to the rutile $c$ axis ($c_R$) and is thus commonly denoted $d_{\parallel}$. The two bands overlap in energy, and the resulting non-zero density of states at the Fermi level accounts for the metallic behavior of the rutile phase [13,18]. **(c)** In the low-temperature ($T<T_{IMT}$) insulating phase the lattice undergoes a structural transition to a lower-symmetry ($P2_1/c$) monoclinic crystal system via dimerization of the neighboring V atoms along the $c_R$ direction and tilting of the resultant V-V dimers along the rutile [110] and $[1\bar{1}0]$ directions. Each dimerized V-V atomic pair shares a singlet electronic state composed of two strongly-correlated V $3d^1$ electrons (shown in blue) [18]. **(d)** V-V dimerization splits the highly-directional $d_{\parallel}$ orbitals into the bonding and anti-bonding bands, and the tilting of the dimers shifts the $\pi^*$ band to higher energies due to the increase of the $p$-$d$ orbital overlap [13,18], together producing an insulating gap of 0.6 eV – the key aspect of the monoclinic phase observed via a wide variety of experimental techniques [25,26]. Additional $d_{\parallel}$ feature in DOS, which arises at the onset of the conduction band (shown in blue) is a unique fingerprint of the strong electron-electron correlations within the dimers [18], accessible experimentally via polarization-dependent XAS at the O $K$ edge (see Ref. 27 and this work). **(e)** Temperature-dependent x-ray diffraction θ-2θ scans across the $TiO_2$ substrate (002) and the $VO_2$ film peaks show a clear structural transition in $VO_2$ manifested by an abrupt change in the inter-planar atomic spacing along the direction normal to the film surface at 295K (inset). Concomitant XRD and electronic transport measurements were collected for the heating cycle, with 1 hour temperature equilibration time between scans. **Inset:** Temperature-dependent resistance (purple circles) and $c_R$ lattice

parameter (green circles) obtained concomitantly via electronic transport and x-ray-diffraction measurement respectively. See full dataset in the supplementary material [23].

**FIG. 2.** **(a)** Schematic diagram of the polarization-dependent XAS measurement geometry used in this study. Linearly-polarized x-rays are incident at 15° to the surface of the coherently-strained epitaxial 10 nm-thick $VO_2/TiO_2(001)$ sample, with the photon polarization set to either parallel ($E \parallel c_R$) or perpendicular ($E \perp c_R$) to the $c_R$ axis (along the sample normal) of the film enabling preferential probing of the strongly-directional $d_\parallel$ ($d_{x^2-y^2}$) and $\pi^*$ ($d_{xz}$ and $d_{yx}$) orbitals depicted in **(b)**, respectively. **(c)** Polarization-dependent O *K* edge XAS measurements of $VO_2$ in the high-temperature ($T=T_{IMT}+15K$) metallic state (shown as open and solid red symbols) and in the low-temperature ($T=T_{IMT}-15K$) insulating state (shown as open and solid blue symbols). Shift of the leading slope of the edge towards lower energy between the insulating and the metallic phases of $VO_2$ corresponds to the collapse of the insulating band gap on the unoccupied side of the energy band diagram (upper gap collapse). Distinct dichroic signal at the onset of the absorption edge in the insulating state presents direct evidence of the additional $d_\parallel$ orbital character at the bottom of the unoccupied conduction band, which is predicted by theory [18] and is shown schematically in Fig. 1(d). **(d)** $d_\parallel$ V-V singlet peak at the onset of the conduction band (528.7 eV) and the $d_\parallel$ Peierls peak at 530.2 eV, both obtained by calculating the $I_\parallel$-$I_\perp$ XAS intensity taken directly from **(c).**

**FIG. 3.** **(a)** Temperature-dependent evolution of the $d_\parallel$ V-V singlet peak intensity (blue/white symbols) showing distinctly different transition temperature ($T_{corr}=290$ K) as compared to the $T_{IMT}$ (295 K), the critical temperature at which the collapse of the upper band gap (red solid symbols) as well as the structural transition (yellow solid symbols) is observed in $VO_2$. Upper gap size is estimated by fitting the edge threshold with a polynomial function and extracting the energy (position along the x-axis) of the half-maximum point from the fitted curve. Error bar analysis is presented in the supplementary material [23]. **(b)-(d)** Schematic representation of the three phases of $VO_2$ implied by the experimental data in the

plots on the left. **(b)** The low-temperature phase ($T \ll T_{IMT}$) is a monoclinic insulator with a strongly-correlated singlet electronic state on each V-V dimer. At $T=T_{corr}$ the strong Coulomb correlations within the dimers soften, giving rise to a new monoclinic insulating phase shown in **(c)** via a purely-electronic phase transition. Finally, only after the *e*-*e* correlations are sufficiently diminished ($T=T_{corr}+3$ K), the system undergoes a transition to a rutile metallic phase shown in **(d).**

# FIG. 1

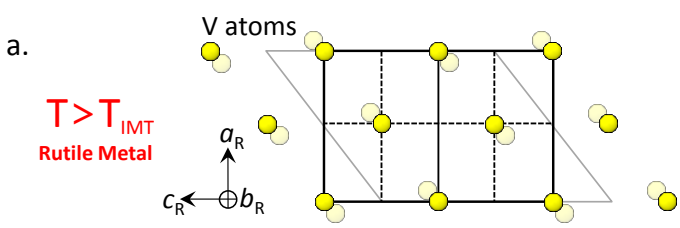
a.
V atoms
T>T IMT
Rutile Metal
a R
c R
b R

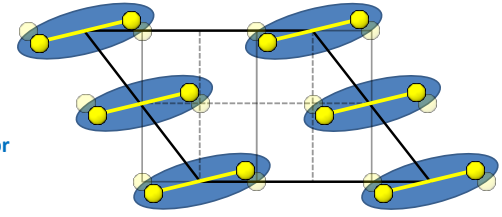
c.
T<T IMT
Monoclinic Insulator

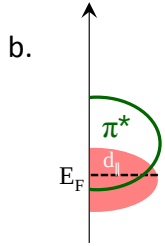
b.
π*
d∥
E F

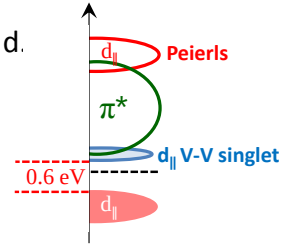
d.
d∥
Peierls
π*
d∥ V-V singlet
0.6 eV
d∥

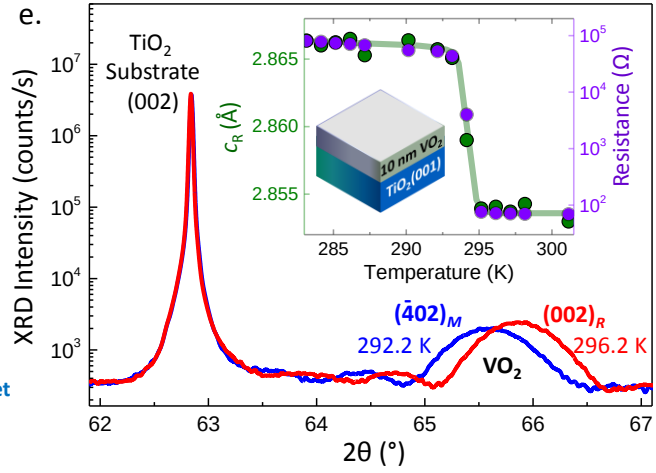
e.
TiO2 Substrate (002)
XRD Intensity (counts/s)
2θ (°)
(4̄02)M
292.2 K
(002)R
296.2 K
VO2
cR (Å)
Resistance (Ω)
Temperature (K)
10 nm VO2
TiO2(001)

FIG. 2

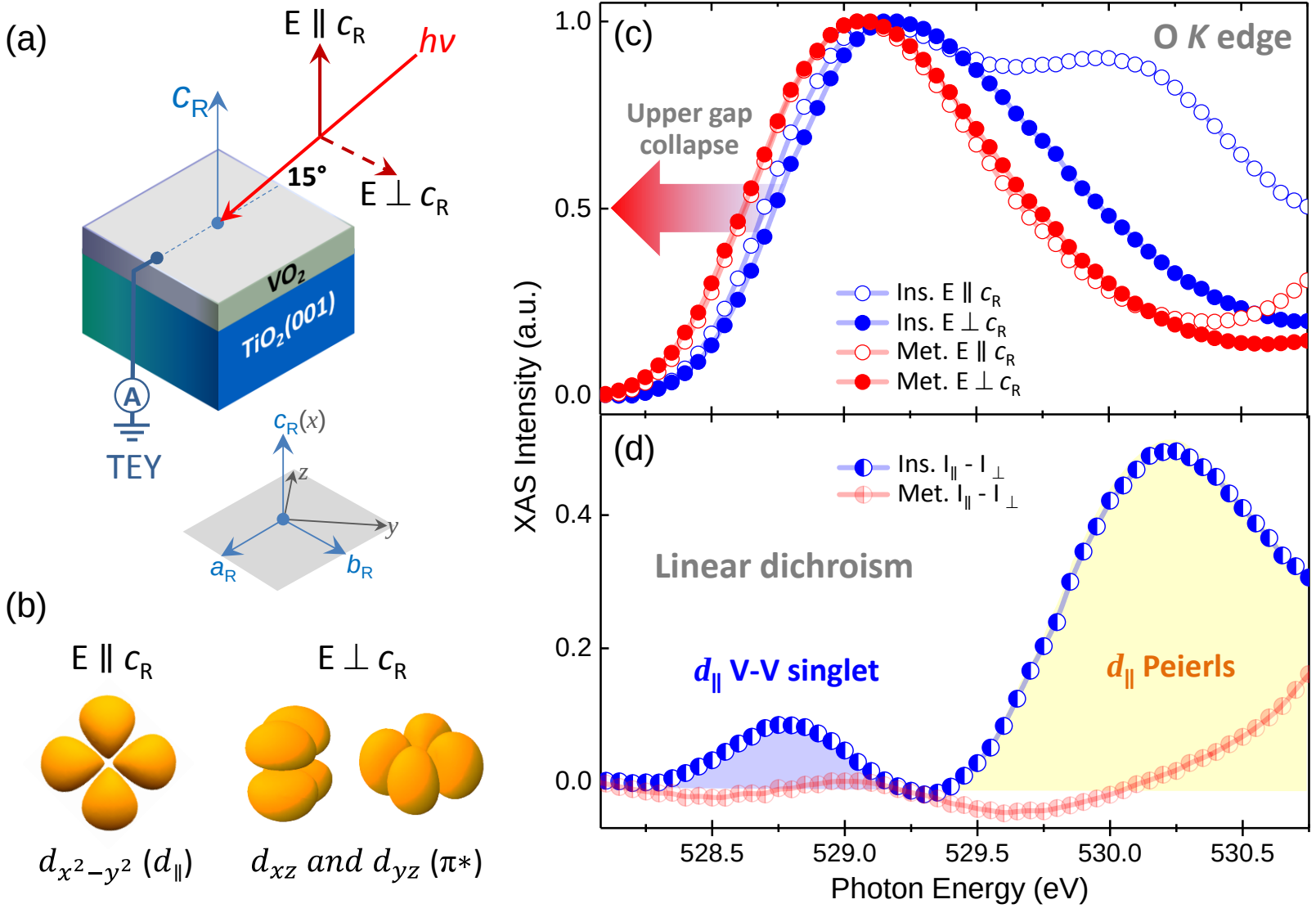
(a)
E ∥ $c_R$
hv
$c_R$
15°
E ⊥ $c_R$
$VO_2$
$TiO_2$(001)
A
TEY
$c_R(x)$
z
y
$a_R$
$b_R$
(b)
E ∥ $c_R$
E ⊥ $c_R$
$d_{x^2-y^2}$ ($d_\parallel$)
$d_{xz}$ and $d_{yz}$ ($\pi^*$)
(c)
O K edge
Upper gap collapse
Ins. E ∥ $c_R$
Ins. E ⊥ $c_R$
Met. E ∥ $c_R$
Met. E ⊥ $c_R$
XAS Intensity (a.u.)
1.0
0.5
0.0
(d)
Ins. $I_\parallel$ - $I_\perp$
Met. $I_\parallel$ - $I_\perp$
Linear dichroism
$d_\parallel$ V-V singlet
$d_\parallel$ Peierls
0.4
0.2
0.0
528.5
529.0
529.5
530.0
530.5
Photon Energy (eV)

FIG. 3

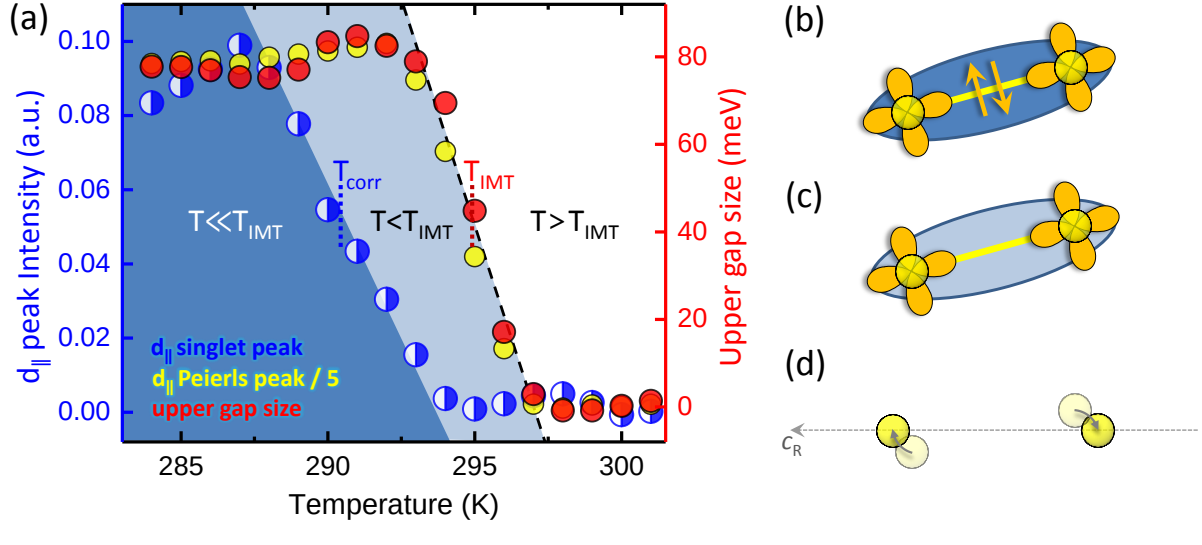
(a)
0.10
0.08
0.06
0.04
0.02
0.00
d∥ peak Intensity (a.u.)
80
60
40
20
0
Upper gap size (meV)
T≪T_IMT
T_corr
T<T_IMT
T_IMT
T>T_IMT
d∥ singlet peak
d∥ Peierls peak / 5
upper gap size
285
290
295
300
Temperature (K)
(b)
(c)
(d)
c_R